Clays and Clay Minerals, Vol. 63, No. 6, 432–442, 2015.

FORMATION AND RESTACKING OF DISORDERED SMECTITE OSMOTIC HYDRATES

Benjamin Gilbert[1,+], Luis R. Comolli[2,+], Ruth M. Tinnacher[1], Martin Kunz[3], and Jillian F. Banfield[1,4,*]

[1] Energy Geoscience Division, Lawrence Berkeley National Laboratory, Berkeley, USA
[2] Life Sciences Division, Lawrence Berkeley National Laboratory, Berkeley, USA
[3] Advanced Light Source, Lawrence Berkeley National Laboratory, Berkeley, USA
[4] Earth and Planetary Sciences, University of California – Berkeley, Berkeley, USA

Abstract—Clay swelling, an important phenomenon in natural systems, can dramatically affect the properties of soils and sediments. Of particular interest in low-salinity, saturated systems are osmotic hydrates, forms of smectite in which the layer separation greatly exceeds the thickness of a single smectite layer due to the intercalation of water. *In situ* X-ray diffraction (XRD) studies have shown a strong link between ionic strength and average interlayer spacing in osmotic hydrates but also indicate the presence of structural disorder that has not been fully described. In the present study the structural state of expanded smectite in sodium chloride solutions was investigated by combining very low electron dose, high-resolution cryogenic-transmission electron microscopy observations with XRD experiments. Wyoming smectite (SWy-2) was embedded in vitreous ice to evaluate clay structure *in aqua*. Lattice-fringe images showed that smectite equilibrated in aqueous, low-ionic-strength solutions, exists as individual smectite layers, osmotic hydrates composed of parallel layers, as well as disordered layer conformations. No evidence was found here for edge-to-sheet attractions, but significant variability in interlayer spacing was observed. Whether this variation could be explained by a dependence of the magnitude of long-range cohesive (van der Waals) forces on the number of layers in a smectite particle was investigated here. Calculations of the Hamaker constant for layer-layer interactions showed that van der Waals forces may span at least five layers plus the intervening water and confirmed that forces vary with layer number. Drying of the disordered osmotic hydrates induced re-aggregation of the smectite to form particles that exhibited coherent scattering domains. Clay disaggregation and restacking may be considered as an example of oriented attachment, with the unusual distinction that it may be cycled repeatedly by changing solution conditions.

Key Words—Clay Swelling, Cryogenic Transmission Electron Microscopy, Montmorillonite, van der Waals Forces.

INTRODUCTION

Despite their widespread importance in soils, sediments, oceans, the atmosphere, and for technological applications, scientific understanding of the behavior of swelling clays, such as smectite, is incomplete (Low and Margheim, 1979; Laird, 2006). Clay swelling influences significantly the structure and permeability of soils and subsurface sediments including clay-rich shales (Anderson *et al.*, 2010). Smectite comprises a variety of 2:1 layer silicates with sufficiently low charge to enable them to swell, accommodating water molecules and organic compounds in the interlayer region (Foster, 1955; Laird, 2006). At elevated temperature and very dry conditions, all interlayer water may be removed. In humid air or high-ionic-strength solutions, smectites can accommodate between 1 and 3 ordered layers of water, forming "crystalline hydrates" with basal spacings that vary in discrete steps from 1.1 to 1.9 nm (Dazas *et al.* 2015).

In low-ionic-strength solutions, smectites can incorporate a much larger amount of water into the interlayer region than would be the case for high-ionic-strength solutions. In this regime, expansion of the clay is driven by an osmotic process (Norrish, 1954) justifying the description of the consequent structured material as "osmotic hydrates" (*cf.* Luckham and Rossi, 1999). In a landmark paper, Norrish (1954) reported that smectite undergoes a discontinuous (first-order) transition from the crystalline to osmotic hydrate state as solution ionic strength is decreased. At concentrations of <~0.25 M NaCl for Wyoming bentonite, the separation between layers shows a linear dependence on $N^{-½}$, where N is the salt concentration. Remarkably, this trend was observed out to periodicities of ~14 nm and was subsequently shown to be a function of salt type and concentration, clay concentration and layer charge, and temperature (Viani *et al.*, 1983; Slade *et al.*, 1991; Zhang *et al.*, 1993; Faisandier *et al.*, 1998; Amorim *et al.*, 2007; Svensson and Hansen, 2013).

* E-mail address of corresponding author:
jbanfield@berkeley.edu
+ Equal co-authors
DOI: 10.1346/CCMN.2015.0630602

https://doi.org/10.1346/CCMN.2015.0630602 Published online by Cambridge University Press

In osmotic hydrates, equilibrium layer-layer separations derive from a competition between repulsive electrostatic forces and attractive van der Waals (vdW) forces between the layers (Laird, 2006). Because both interactions are reduced by the shielding effect of interlayer ions, the interlayer spacing exhibits the observed dependence on ionic strength. The same concepts underpin the theory of colloid dispersions predicted by the theory of Derjaguin and Landau, Verwey and Overbeek (DLVO), and hence many treatments of this regime apply DLVO theory (Greathouse *et al*., 1994; Liu, 2013). For smectite with low structural charge (such as montmorillonite) and monovalent ions, these approaches can reproduce trends in interlayer spacing with ionic strength. For example, Quirk and Marčelja (1997) showed DLVO theory to correctly predict the interlayer separation of Li-montmorillonite from 1.8 to 12 nm as a function of pressure and LiCl concentration. DLVO failed, however, to predict accurately the ionic-strength threshold for aggregation (Missana and Adell, 2000) and swelling pressure (Viani *et al.*, 1983). Moreover, all models based on DLVO theory fail to depict accurately behavior for highly charged surfaces or non-monovalent ions such as Ca^{2+} (Kleijn and Oster, 1982).

All XRD and small-angle X-ray scattering (SAXS) studies of smectite osmotic hydrates show evidence of disorder in the interlayer spacings (Quirk and Marčelja, 1997; Faisandier *et al.*, 1998). Whether this is caused by intrinsic heterogeneity of natural smectites, with cation substitutions leading to local variations in layer charge, or whether it is simply a consequence of natural fluctuations due to, *e.g.* Brownian motion, is not known. Molecular simulations have predicted that alternative stacking configurations, such as edge-to-face, could prevail under certain conditions (Jönsson *et al.*, 2008). Tests of such predictions are currently lacking, however.

The present authors suggest that osmotic hydrates contain structural disorder that has not been fully characterized by any prior study and that a better understanding of this disorder would advance knowledge of the forces between clay layers. Conventional methods are unable to reveal detailed information about hydrated smectite structure. Despite recent advances in the analysis of X-ray scattering data, this approach has limited the ability to characterize disorder in suspensions of anisotropic crystallites. Accurate quantification of the distributions of different layer hydration states in crystalline hydrates is possible from XRD data (Pons *et al*., 1981; Ferrage *et al.*, 2005; Dazas *et al.*, 2015), but not the distributions of spacings in osmotic hydrates. Even fewer attempts have been made to quantify disorder in osmotic hydrates. Several groups have used SAXS to explore the average distances between layers in completely exfoliated smectite as a function of solution conditions (*e.g.* Paineau *et al.*, 2011). Interpretation of SAXS data beyond quantification of mean interlayer spacings is very model dependent, however, and direct observations of layer disorder, useful for validating proposed models, have not been reported to date.

Only transmission electron microscopy (TEM) has the necessary spatial resolution for imaging smectite particles. Guthrie and Veblen (1989) showed that it was possible to measure coherent stacking sequences in mixed-layer illite-smectite. The ultrahigh vacuum conditions required for TEM can cause complete loss of interlayer water, however. Many groups have studied smectites that were expanded by alkylammonium intercalation and preserved in epoxy (*e.g.* Schumann *et al.*, 2014) but epoxy intrusion into the interlayers can alter interlayer spacing relative to values observed by XRD for hydrated systems. These conventional TEM methods are even less suitable for studying osmotic hydrates.

Here a first imaging study of smectite in the osmotic hydrate state using cryogenic transmission electron microscopy (cryo-TEM) is reported. Rapid vitrification of samples enabled electron microscopy imaging of particles in aqueous suspensions. The flash freezing approach has been proven to preserve the structure of hydrated biological macromolecules such as ribosomes for which independent atomic-resolution structures exist (see Cheng, 2015, and references therein). Cryo-TEM has been used previously to determine the structure of microbial mineral precipitates (Comolli *et al.*, 2011) and the structure of fragile, extended aggregates of Fe oxyhydroxide nanoparticles (Yuwono *et al.*, 2010; Frandsen *et al.*, 2014; Legg *et al.*, 2014). Cryo-TEM was used by Segad *et al.* (2012) to compare the aggregate structures of Na- and Ca-equilibrated montmorillonite suspensions, but without investigating the osmotic hydrate regime.

In the current study a state-of-the-art low-dose cryo-TEM was used to characterize osmotic hydrates formed by a montmorillonite from a Wyoming bentonite (SWy-2). The bentonite was either studied without treatment, or was treated with standard methods to obtain a purified, Na-equilibrated montmorillonite fraction of sub-2 μm particles. Image details led the authors to speculate that variations in interlayer spacings arise neither from intrinsic layer charge heterogeneity nor from random Brownian motion, but rather from the action of vdW forces which extend over multiple interlayer distances. This length scale is not typically considered in theories of smectite swelling. Because configurational disorder prevented direct validation of this concept in the present study, the idea was tested using a recently developed computational method for prediction of vdW forces in multi-layer geometries. Despite lack of the materials-properties data required for accurate predictions for layered aluminosilicates in high-salinity solutions, calculations in the present study suggest strongly that equilibrium interlayer spacings in osmotic hydrates are influenced by layer–layer vdW forces that extend across multiple smectite layers.

https://doi.org/10.1346/CCMN.2015.0630602 Published online by Cambridge University Press

MATERIALS AND METHODS

Experimental methods

Clay treatments. The experiments used samples of the Source Clay SWy-2 from the Source Clays Repository of The Clay Minerals Society (http://www.clays.org/SOURCE%20CLAYS/SCBackground.html). SWy-2 is a Na-rich bentonite from Crook County, Wyoming, in which the smectite fraction is montmorillonite. A multistep treatment of this material was performed to create a homoionic Na-saturated suspension free of mineral impurities referred to as Na-montmorillonite. The steps are described in more detail in the Supplementary Information section (deposited with the Editor in Chief and available at http://www.clays.org/JOURNAL/JournalDeposits.html), and included (1) the removal of calcite impurities using a 1 M sodium acetate/0.564 M glacial acetic acid solution, (2) the equilibration of the clay with a 1 M sodium chloride solution, (3) the removal of excess Na-salts with Nanopure water, (4) the separation of quartz and feldspar impurities from clay particles by centrifugation while retaining the <2 μm fraction, and (5) oven drying of the purified clay mineral phase at 45ºC (~2 weeks). Steps 1−3 were performed by dialysis. The dried clay was recovered and ball milled for 2 min and stored dry until its resuspension in NaCl solutions.

Dried smectite was pressed into powder pellets, carbon coated, and analyzed by electron probe microanalysis (EPMA) with a Cameca SX-51 in the Department of Earth and Planetary Science at the University of California, Berkeley, USA. Data acquisition, analysis, and correction procedures were conducted with the software, *Probe*, for EPMA, as described in the Supplementary Information section.

Cryo-TEM specimen preparation and instrumentation. As-received or treated samples of dried and powdered Wyoming montmorillonite were suspended in water or NaCl solutions at salt concentrations below the crystalline-to-osmotic transition threshold (~0.25 M). Samples were equilibrated overnight. Aliquots of 5 μL were taken directly from the suspensions, placed onto 200 mesh lacey carbon formvar or 300 mesh lacey carbon Cu-grids (Ted Pella, Incorporated, California, USA, #01881 and #01895, respectively), blotted manually with filter paper and plunged into liquid ethane at liquid nitrogen temperature. The TEM grids had previously been glow discharged.

Images were acquired on a JEOL-3100-FFC electron microscope equipped with a field emission gun (FEG) electron source operating at 300 kV, an Omega energy filter, and a cryo-transfer stage. Images were recorded on a Gatan 795 4k × 4k charge-coupled device (CCD) camera (Gatan Inc., Pleasanton, California, USA) mounted at the exit of an electron decelerator operated at 200 kV, resulting in images formed by a 100 kV electron beam at the CCD. The stage was cooled to 80 K with liquid nitrogen during the acquisition of all data sets.

Cryo-TEM image acquisition and analysis. Over 100 two-dimensional (2D) images were recorded at nominal magnifications of 50 k×, 80 k×, 120 k×, and 200 k× giving pixel sizes of 0.112 nm, 0.07 nm, 0.047 nm, and 0.028 nm at the specimen, respectively. Underfocus values ranged between ~1000 ± 100 nm and 35 ± 5 nm (measured from minimum contrast), and energy filter widths were typically ~30 eV. The survey of the grids and the selection of suitable targets were done in low-dose defocused diffraction mode to minimize radiation damage, as established for biological samples (Luef *et al.*, 2012). Images were acquired under low-dose conditions, typically with doses of ~125−250, 320, 720, and 1000 e^{-} $Å^{-2}$ per image for nominal magnifications of 50 k×, 80 k×, 120 k×, and 200 k×. The software *ImageJ* 1.38x, National Institutes of Health (NIH, http://rsb.info.nih.gov/ij/) was used for analysis and measurements of the 2D image projections.

X-ray diffraction. Powdered samples of treated SWy-2 were suspended in NaCl solutions or ultrapure water at a smectite concentration of 200 mg/mL for 1 week. A small aliquot of the suspensions was placed in 300-μm internal-diameter quartz capillaries for synchrotron XRD analysis at beamline 12.3.2 at the Advanced Light Source. For improved powder statistics, samples within the capillary were scanned over a 100 μm × 100 μm (5 μm steps) area through a 2 × 10 μm 10 keV beam, equivalent to a wavelength of 1.2398 Å. Powder patterns were recorded in 600-s exposures using a Pilatus-1M area detector (Dectris, Baden-Dättwil, Switzerland) positioned at 20º2θ and ~190 mm distance. The experimental geometry was calibrated using Al_2O_3 National Institutes of Standards and Technology (NIST) standard material (SRM 676a). Initial suspensions were too dilute to provide either interlayer or in-plane diffraction peaks, so the capillaries were spun at 10 krpm for 2 h in a special insert machined to fit an Eppendorf centrifuge. Centrifugation caused a visible increase of clay density in the salt suspension and permitted analysis by XRD. A portion of the same sample was dried on a filter, removed gently and re-powdered, and placed into an identical capillary. The low-angle (1.8−8º2θ) data were processed by fitting and removing an exponential function corresponding to scattering from water. The wide-angle (5−35º2θ) data were processed by subtracting the scattering from an empty capillary.

Calculations

Van der Waals force calculation. The freely available *Gecko Hamaker* code (Rajter *et al.*, 2013) was used for simulating the vdW interactions within multi-layered models of stacked smectite in water. The *Gecko* code calculates the Hamaker constant A_{123} for the interaction

https://doi.org/10.1346/CCMN.2015.0630602 Published online by Cambridge University Press

between two structured objects 1 and 3 separated by medium 2 of thickness D. The approach was described fully by Podgornik and Parsegian (2004) and Parsegian (2006) and is based upon the theory of Lifshitz (1956) that links the complex optical properties of two solids to the dispersion forces between them. The vdW force per unit area, P_{vdW}, is then calculated from:

$$P_{vdW} = \frac{A}{6\pi D^3}$$

A series of calculations was designed to test the hypothesis that long-range vdW interactions (beyond next-nearest neighbor layers) made a significant contribution to the overall cohesion energy of a smectite particle with a uniform interlayer spacing that was fixed at either 4 or 5 nm. Given the lack of optical-property measurements for layer silicates, a silica-corundum-silica stack was used to approximate one individual 2:1 layer, using material constants for corundum (Al_2O_3) and amorphous silica (SiO_2) from the *Gecko* database (French *et al*., 1998; Tan *et al*., 2005). A full calculation of clay particle cohesion energy as a function of all relevant parameters will require new dielectric measurements for layer silicates and for salt solutions.

The Hamaker constant for inner- and outermost pairs of clay layers was calculated as a function of the total number of layers in a clay particle, from 2 to 14. For these calculations the intervening solution was pure water because the dielectric functions for electrolyte solutions are not known accurately. A portion of the vdW forces are screened effectively by electrolyte solutions, but the most significant part involves electronic fluctuations which occur on a timescale that is far too short to be effectively screened by the motion of ions in solution (Davies and Ninham, 1972). No previous study of ionic-strength effects on vdW interactions between minerals could be found by the present authors. However, Marra (1985) showed that the strength of vdW interactions between digalactosyl-diglyceride bilayers decreased by ~50% in 0.2 M NaCl compared to water. Therefore, the 0.1 M solution used in the present study was assumed to reduce the vdW strength by half relative to that predicted for pure water. This correction factor was not applied to the calculations.

Electrostatic force calculation. For comparison with the magnitude of the vdW interaction forces, the electrostatic repulsion pressure between two model 'montmorillonite' layers in 0.1 M NaCl was calculated. The pressure, P_{EDL}, was calculated from the force between overlapping electrical double layers (EDL):

$$P_{EDL} = \frac{1}{2}\varepsilon_r\varepsilon_0\kappa^2\Phi_0^2\left(\frac{1}{\cosh\frac{\kappa D}{2}}\right)^2$$

where $\kappa = (\varepsilon_r\varepsilon_0 RT/2z^2F^2c)^{1/2}$ is the inverse Debye length, $\varepsilon_r\varepsilon_0$ is the dielectric permittivity of water, R is the ideal gas constant, T = 298 K is temperature, z = 1 is the ionic valence, F is Faraday's constant, and c is the bulk electrolyte concentration (in ions/cm^3). The surface potential, Φ_0, was fixed at 250 mV (Miller and Low, 1990; Hou *et al*. 2009).

RESULTS

Both intact and treated SWy-2 formed visually clear suspensions readily after equilibration in 0.1 M NaCl solution at smectite concentrations of 50 mg/mL or lower. Representative low-magnification defocused diffraction imaging of cryo-TEM preparations are shown in Figures S1–S3 (deposited with the Editor in Chief and available at http://www.clays.org/JOURNAL/JournalDeposits.html). The suspensions contained a dispersion of individual layers consisting of one octahedral and two tetrahedral sheets (2:1 layers), the fundamental structural unit of smectite, and particles containing multiple stacked 2:1 layers (smectite particles). Higher-magnification lattice-fringe images captured individual layers, smectite particles, and osmotic hydrates that lay within the depth of focus in the vitreous ice sample (estimated to be >100 nm for 80 k× magnification). These images revealed that the majority of smectite in both the untreated and treated clays had expanded beyond all crystalline hydrate states and formed osmotic hydrates, as expected for the low NaCl concentrations. All images revealed conformational disorder including heterogeneity in smectite layer spacings.

An image recorded from a suspension of untreated SWy-2 illustrates the tendency of the expanded smectite to form oriented, parallel stacking configurations in the osmotic hydrate state (Figure 1a). In other cases, despite the formation of pairs or triplets of parallel smectite layers, these units were rotated with respect to each other within the larger ensemble (Figure 1b). Partial osmotic hydrates that also include regions of crystalline hydrates with interlayer spacings consistent with both two- and three-water layers are shown in Figure 2. Completely delaminated individual clay layers with little evident curvature were also observed (Figure S4) as were highly disordered aggregates of layers (Figure S5).

The treated SWy-2 sample delaminated more completely than the untreated sample following equilibration with 0.1 M NaCl solutions. More individual layers were observed and no examples of crystalline hydrates were found. As shown in Figure 3, the expanded smectite was frequently observed as parallel, stacked layers, just as observed for untreated SWy-2 suspended in 0.1 M NaCl. Fully delaminated layers, either with evident curvature or with a highly linear morphology, were observed (Figure S6). Also observed were disordered osmotic hydrates (Figure S7A) and parallel assemblies rotated relative to one another (Figure S7B), as seen for the untreated sample.

https://doi.org/10.1346/CCMN.2015.0630602 Published online by Cambridge University Press

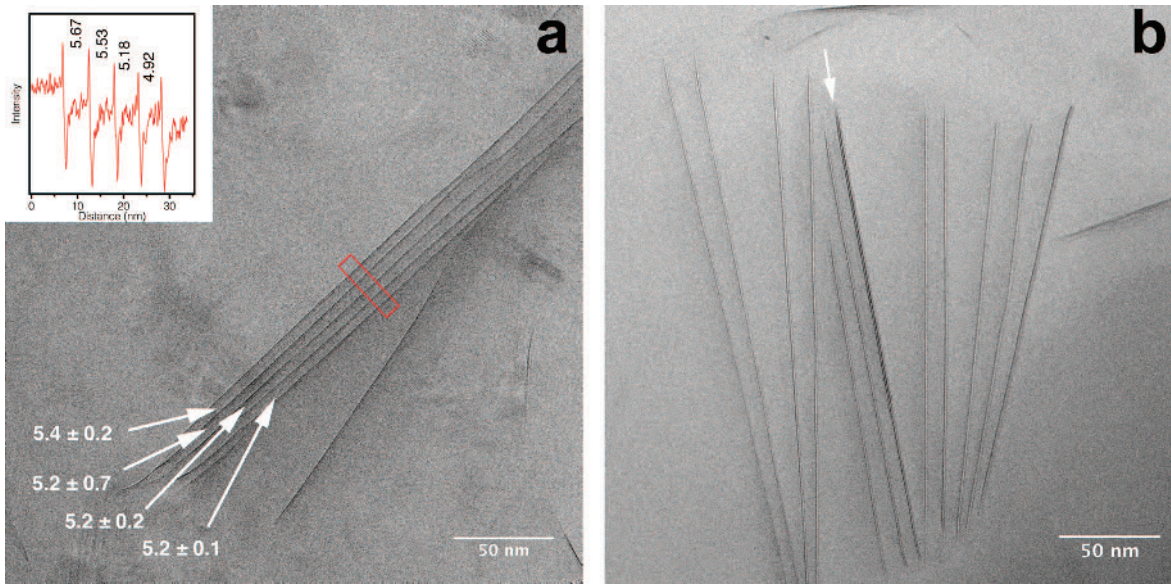


Figure 1. Cryo-TEM images of untreated SWy-2 smectite, 50 mg/mL equilibrated in 0.1 M NaCl solution. (a) Example of a more ordered stacking configuration in the osmotic hydrate state showing the average interlayer spacing and the standard deviation (nm) from five measurements along the osmotic hydrate (*cf.* Figure S9). Inset: example intensity profile from one indicated area used to determine interlayer spacing (nm). (b) Example of a partially ordered stacking configuration. The arrow indicates a pair of layers in a crystalline hydrate configuration.

As shown by the EMPA data (Table S1, deposited with the Editor in Chief and available at http://www.clays.org/JOURNAL/JournalDeposits.html), the long dialysis period decreased slightly the Si:Al

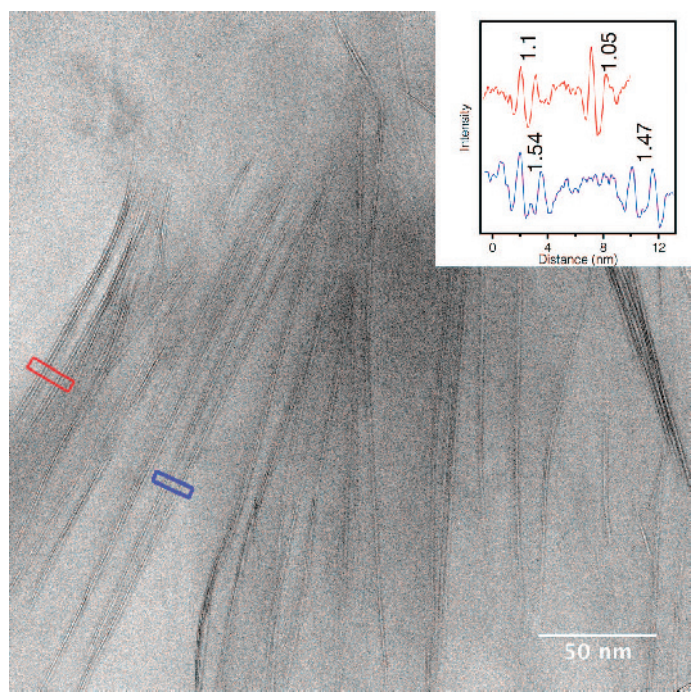


Figure 2. Cryo-TEM image of untreated SWy-2 smectite, 50 mg/mL equilibrated in 0.1 M NaCl solution. The image shows evidence of a partially expanded osmotic hydrate that incorporates 2- and 3-water crystalline hydrates. Inset: intensity profiles from the areas indicated reporting the interlayer spacing (nm).

https://doi.org/10.1346/CCMN.2015.0630602 Published online by Cambridge University Press

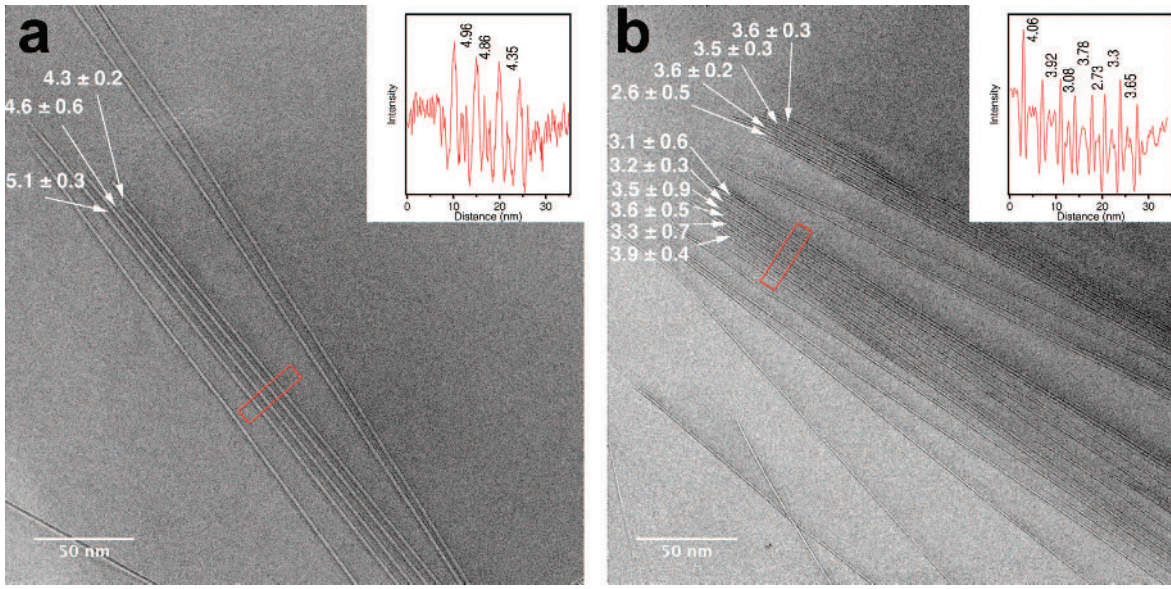


Figure 3. Cryo-TEM images of treated SWy-2 smectite, 200 mg/mL equilibrated in 0.1 M NaCl solution. Also given are the average interlayer spacing and the standard deviation (nm) from five or eight measurements along the osmotic hydrate. Insets: example intensity profiles from the regions indicated used to estimate interlayer spacing (nm).

ratio. This could be an indication of smectite dissolution and the release of Al^{3+} ions that are known to be able to displace Na^{+} from the interlayer regions. Extensive release of trivalent Al ions would be expected to collapse the smectite, however, which was not observed.

For smectite particles that showed the expected osmotic hydrate structure, the interlayer spacings were measured. Because the smectite layers are oriented at an unknown tilt with respect to the image plane, such measurements could overestimate the interlayer spacing. For example, the TEM asymmetric intensity profile shown in Figure 1a probably indicates tilt of the layers. As shown in Figure S8, however, analysis of a tilt series showed that a lattice-fringe imaging condition exists only for tilt angles within ±15º or less of the beam direction. Thus, the measured spacings could be up to 5% too large.

The mean interlayer spacings obtained from ordered osmotic hydrates (Figures 1–3), along with the standard deviations determined from 5 to 8 measurements at ~50-nm intervals (Figure S9) revealed a significant range of interlayer spacings (from 2.6 to 5.4 nm). Although the sample size was very small, the different clay particles in the same sample exhibited different average spacings. One plausible hypothesis is that the stoichiometric composition of the clay (and hence layer charge) was locally homogeneous but varied throughout the sample. The observations suggested an alternative hypothesis, however: the mean interlayer spacing could be a function of the number of layers in the particle if vdW interactions extend beyond a single interlayer distance. Thus, a series of numerical calculations, designed to test the idea that long-range vdW interactions could significantly alter the cohesion energy of a stack of 2:1 layers, was performed.

The calculations of the vdW interactions between pairs of model 2:1 layers in an osmotic hydrate (Figure 4 inset) assumed pure water in the interlayer space because accurate dielectric functions for NaCl solutions were not available. As discussed above, the NaCl probably reduces the strength of the vdW interactions by ~50% relative to pure water (Marra, 1985). Because no accurate measurement of vdW shielding for saline solutions currently exists, however, no correction factor was applied to the calculations reported in Figure 4. Although the effect of salinity on the absolute magnitude or range of the vdW interaction forces is not known precisely, this uncertainty does not invalidate the calculation, which aimed to test the dependence of vdW interactions on layer number.

The calculations of layer–layer attraction, P_{vdW}, summarized in Figure 4, clearly predict that the vdW interaction forces between a pair of model clay layers in a particle are affected by the presence of additional layers. For pure water and a fixed spacing of 4 nm, the results predict that long-range interactions increase the total cohesion energy of the system by >10%. Beyond ~5 layers, vdW interactions contribute little and, thus, can be ignored. An estimate of the electrostatic repulsion pressure, P_{EDL}, for a pair of smectite layers in 0.1 M NaCl, separated by 4 nm, is shown in Figure 4. At equilibrium, P_{vdW} and P_{EDL} should be equal and opposite. This equality is approximately satisfied if the 0.1 M NaCl shields half of the vdW contribution as indicated by the results of Marra (1985).

https://doi.org/10.1346/CCMN.2015.0630602 Published online by Cambridge University Press

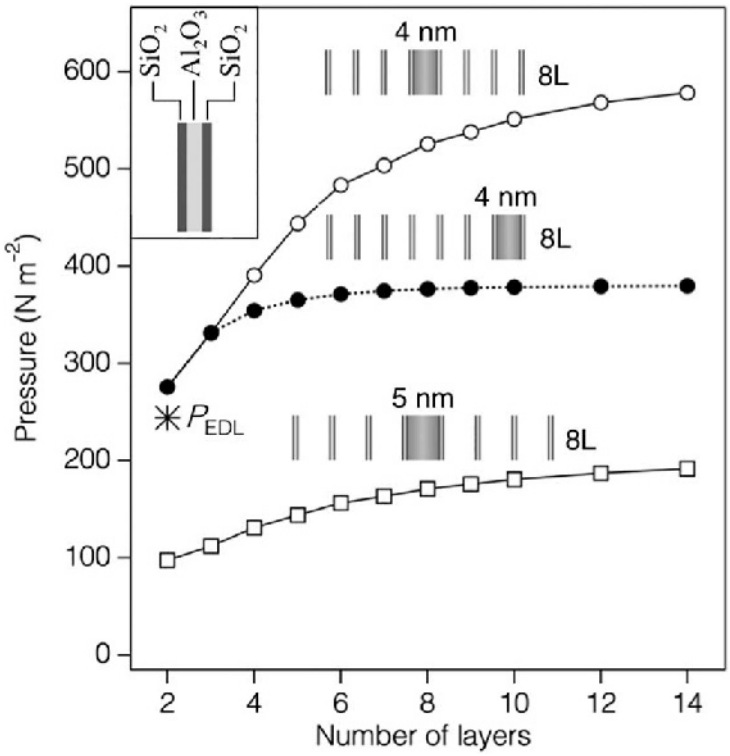


Figure 4. The calculated van der Waals force per unit area between one pair of smectite layers in water as a function of the total number of layers in a stack. A single 2:1 layer (composed of tetrahedral-octahedral-tetrahedral sheets) was represented by a silica-corundum-silica multilayer (inset). Calculations were performed for the centermost (open symbols) and outermost (solid symbols) pair of layers and for interlayer spacings of 4 nm (circles) and 5 nm (squares). Illustrations of the geometry are depicted for 8-layer (8L) stacks, with the selected interlayer shaded. Also shown is the electrostatic repulsion pressure (P_{EDL}) calculated for a single pair of 2:1 layers with a surface potential of 250 mV at a separation of 4 nm.

The XRD data acquired from a suspension of treated SWy-2 in 0.1 M NaCl in a capillary and from a portion of the same suspension under filtration are compared in Figure 5. Under fully hydrated conditions, interlayer diffraction peaks with spacings up to 4 nm were not detectable (see figure inset). Thus, although clay particles with spacings in this range were observed from the cryo-TEM, the observed disorder broadened and weakened the scattering. Following filtration and drying, however, the clay exhibited strong (001) and (004) spacings, consistent with one water layer crystalline hydrate containing Na (Wilson *et al.*, 2004).

DISCUSSION

Smectite structure in aqueous solution

The cryo-TEM observations of lattice-fringe spacings for the hydrated smectite structure are in fair agreement with previous XRD data, supporting the present conclusion that the flash-freezing approach did not introduce artifacts. Specifically, the measured interlayer spacings, which range from 2.6 to 5.4 nm, are close to the values reported for hydrated Na-montmorillonite by Zhang *et al*. (1995) but are lower than values reported by Norrish (1954) and Amorim *et al.* (2007). The observation of expanded smectite with a range of interlayer spacings is in agreement with prior inferences based on XRD (Pons *et al.*, 1981; Amorim *et al*., 2007). The imaging results add considerable new insight into the structure and disorder in smectite osmotic hydrates, however.

Montmorillonite possesses a fixed negative charge in the octahedral sheet and reactive oxygen sites at layer edges that are expected to be protonated and positively charged in circumneutral solutions (Bailey, 1988; Tournassat *et al*., 2004). These features have motivated predictions of "house-of-cards" or "overlapping-coins" structures (van Olphen, 1977; Jönsson *et al.*, 2008; Delhorme *et al*., 2011). Despite the considerable disorder, no evidence was observed for such arrangements.

In the present study, smectite 2:1 layers, either in free solution or stacked in particles, typically exhibited less overall curvature (on the 100-nm and longer scale) than observed for expanded smectite imaged in epoxy (*e.g.* Schumann *et al*., 2014). Only one image provided evidence of curvature in isolated layers (Figure S6). Flash freezing is expected to introduce fewer structural artifacts than epoxy-based sample preparations; the present observations are assumed, therefore, to depict accurately the real planarity of hydrated smectite layers. Close inspection of the images, as well as quantitative

https://doi.org/10.1346/CCMN.2015.0630602 Published online by Cambridge University Press

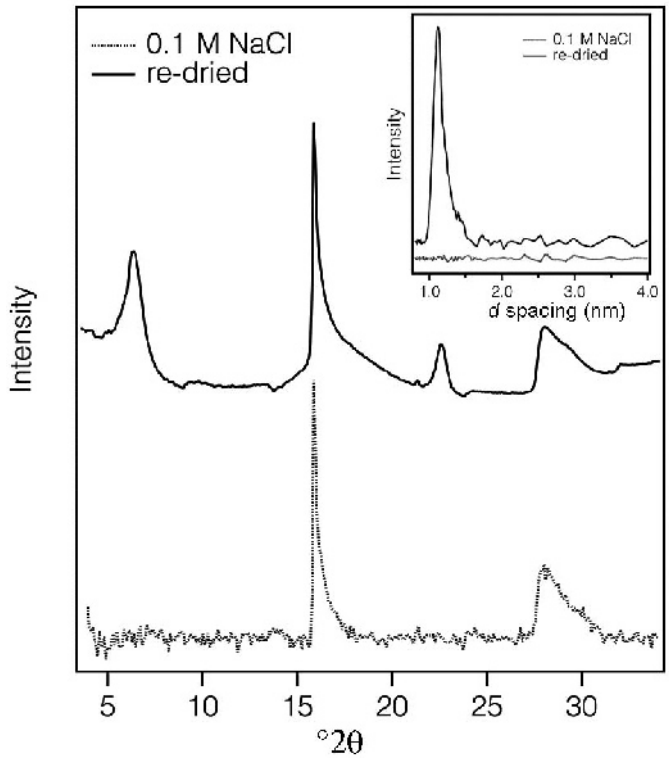


Figure 5. XRD data (5−35º2θ) for treated SWy-2 smectite measured in aqueous suspension in 0.1 M NaCl (lower) and following drying (upper). Inset: low-angle scattering regions (1.8−8º2θ) plotted using the *d*-spacing scale. X-ray wavelength was 1.2389 Å.

measurements of the parallelism of the ordered stacking arrangements (Figure S9), revealed fine-scale undulations in most layers. These undulations could be a consequence of metal substitutions within the layers, but higher-resolution studies will be required to explore this possibility fully.

In many images, one or more layers were observed close to, but not parallel to, layers in an ordered osmotic hydrate particle. Brownian motion is suggested here to result in osmotic hydrates that are in a state of dynamic formation and disassembly. This cannot be tested by cryo-TEM, which captures snapshots of instantaneous structure, or by conventional SAXS methods which provide measurements averaged over many particles and over a significant acquisition time. Fluid-cell TEM might allow the dynamic structure of osmotic hydrates to be observed. The present authors predict that the structural configurations observed by cryo-TEM will enable new models for scattering from disordered lamellar systems to be developed which will allow SAXS analysis of bulk solutions to provide richer and statistically more significant analysis of smectite suspensions.

Long-range attractive interactions spanning multiple smectite layers

The present calculations predict that vdW interactions spanning multiple 2:1 and water layers is a non-negligible contribution to the cohesion of expanded smectite particles. The uncertainties in the magnitudes of the vdW forces described above do not affect this important calculation-based prediction. Long-range vdW interactions must be important in osmotic hydrates because structures with large (*i.e.* >10 nm) layer distances are stabilized. To the best of the authors' knowledge, however, no prior experimental or theoretical study of osmotic hydrates has considered the role of long-range, next-nearest-neighbor vdW interactions. This prediction may be important because it implies that the overall cohesion energy of expanded clay particles is a function of the number of layers in the particle and that the interlayer spacing will be smaller for particles with a larger number of layers. Thus, models of clay swelling based on a single pair of layers (*e.g.* Liu, 2013), or considering only next-layer interactions (*e.g.* Kleijn & Oster, 1982), will underestimate the layer-normalized cohesion energy of larger particles and overestimate the layer distances.

Layer re-association and constraints for attachment-based crystal growth

The XRD data in Figure 5 show clearly that disordered, expanded clay layers, which exhibit no detectable 00l scattering, re-aggregate readily when the water activity is reduced by drying to form ordered crystalline hydrates with strong diffraction perpendicular to the layer plane. Because transformation of osmotic to

https://doi.org/10.1346/CCMN.2015.0630602 Published online by Cambridge University Press

crystalline hydrates involves assembly of individual smectite 2:1 layers in solution, it can be classified as an example of oriented attachment-based crystal growth (OA) (Penn and Banfield, 1998). Such OA has been reported as a crystal-growth mechanism for many poorly soluble nanoparticulate minerals, including oxides and sulfides (Penn *et al*., 2001; Huang *et al*., 2003), and has been observed in suspensions of nanoparticles with a range of morphologies (Yuwono *et al*., 2010; Frandsen *et al*., 2014). The case of assembly of 2:1 smectite layers is distinct from other growth processes described as OA because the attachment process is readily reversible due to the unusually low strength of layer−layer interactions (because attachment does not involve the formation of covalent or ionic bonds). The authors here do not mean to imply that smectite particles form originally through the stacking of individual 2:1 layers that nucleate homogeneously in solution (although this sometimes may be the case). Rather, the 2:1 layer assembly is described as one of the steps in the dynamic process of swelling, disaggregation, and re-aggregation that probably occurs innumerable times over the 'lifetime' of smectite particles.

In research on OA-based crystal growth, the nature of nanoparticle interactions in aqueous solution and the distances over which they interact are uncertain. *In situ* fluid-cell TEM observations of OA-based crystal growth of ferrihydrite indicate the operation of long-range particle–particle interactions (Li *et al*., 2012). Studies of smectite swelling and restacking can provide insights into interparticle forces involved in OA-based crystal growth because the two-dimensional geometry enables interactions that are parallel and normal to the 2:1 layers to be resolved. Observations of attractive forces in the 3 to >20 nm range in expanded clays indicate that particle−particle interactions can occur over such distances (although nanoparticle size and morphology will affect interaction distances).

In OA-based growth, an orienting force is suspected to align nanoparticles as they approach so that interface elimination can yield a single crystal (Li *et al*., 2012; Zhang and Banfield, 2014). Cryo-TEM images show that separated smectite layers in ordered particles are parallel to each other. This geometry is explained conceptually by DLVO theory in which the balance between attractive and repulsive forces orients the surfaces. The cryo-TEM data also show that layers tend to overlap each other. This implies that lateral forces parallel to the 2:1 layers in the osmotic hydrate are sufficiently strong to drive the system to an energy minimum in which the layers superimpose. Attractive layer−layer vdW forces could provide the driving force for this alignment, although electrostatic forces must play a role once the layers are close enough that the electrical double layers overlap. Cryo-TEM observations of smectite *in aqua*, thus, provide insight into the nature of layer−layer interactions controlling clay expansion and restacking and can inform an understanding of related colloidal phenomena including OA-based crystal growth.

CONCLUSIONS

Cryo-TEM observations of flash-frozen suspensions of smectite in 0.1 M NaCl solution revealed that osmotic hydrates, composed of highly planar and close to parallel 2:1 layers, coexisted with 2:1 layers in a range of disordered conformations, but without evidence of alternative edge-to-sheet interactions. The large range of interlayer spacings measured in the osmotic hydrates suggested a role for long-range attractive van der Waals interactions in determining equilibrium structure. Calculations of van der Waals forces in a multi-layer model of expanded smectite predicted that attractive forces acting over at least four smectite interlayers will influence osmotic hydrate cohesion energy. Due to the disorder in the expanded state, (001) diffraction peaks were not detectable in XRD data, but were observed following restacking (through drying). Assembly of individual smectite 2:1 layers in solution can be classified as an example of oriented attachment-based (OA) crystal growth. Further elucidation of the forces that act to align smectite particles during stacking, aided by cryo-TEM observations, will improve understanding of both clay swelling and OA-based growth.

ACKNOWLEDGMENTS

The authors thank Sean Mulcahy for performing electron beam microprobe analysis and Dr Roger French for access to and assistance with the *Gecko Hamaker* code. This work was supported by the Office of Science, Office of Basic Energy Sciences (BES), Chemical Sciences, Geosciences, and Biosciences Division, of the U.S. Department of Energy (DOE) under Contract No. DE-AC02-05CH11231. RMT was supported by the U.S. Department of Energy Used Fuel Disposition (UFD) Campaign, Contract No. DE-AC02-05CH11231. The *Gecko Hamaker* code was developed with support from DOE BES Materials Science and Engineering Division, Biomolecular Materials (BMM) under award DE-SC0008068.

REFERENCES

Amorim, C.L.G., Lopes, C.L.G., Barroso, R.C., Queiroz, J.C., Alves, D.B., Perez, C.A., and Schelin, H.R. (2007) Effect of clay–water interactions on clay swelling by X-ray diffraction. *Nuclear Instruments and Methods in Physics Research A*, **580**, 768−770.

Anderson, R.L., Ratcliffe, I., Greenwell, H.C., Williams, P.A., Cliffe, S., and Coveney, P.V. (2010) Clay swelling − a challenge in the oilfield. *Earth-Science Reviews*, **98**, 201−216.

Bailey, S.W. (1988) *Hydrous Phyllosilicates (exclusive of Micas)*. Reviews in Mineralogy, **19**, Mineralogical Society of America, Washington, D.C.

Cheng, Y. (2015) Single-particle cryo-EM at crystallographic resolution. *Cell*, **161**, 450−457.

Comolli, L.R., Luef, B., and Chan, C.S. (2011) High-resolution 2D and 3D cryo-TEM reveals structural adaptations of two

https://doi.org/10.1346/CCMN.2015.0630602 Published online by Cambridge University Press

stalk-forming bacteria to an Fe-oxidizing lifestyle. *Environmental Microbiology*, **13**, 2915–2929.
Davies, B. and Ninham, B.W. (1972) Van der Waals forces in electrolytes. *Journal of Chemical Physics*, **56**, 5792–5801.
Dazas, B., Lanson, B., Delville, A., Robert, J.L., Komarneni, S., Michot, L.J., and Ferrage, E. (2015) *Journal of Physical Chemistry C*, **119**, 4158–4172.
Delhorme, M., Jönsson, B., and Labbez, C. (2011) Monte Carlo simulations of a clay inspired model suspension: The role of rim charge. *Soft Matter*, **8**, 9691–9704.
Faisandier, K., Pons, C.H., Tchoubar, D., and Thomas, F. (1998) Structural organization of Na- and K-montmorillonite suspensions in response to osmotic and thermal stresses. *Clays and Clay Minerals*, **46**, 636–648.
Ferrage, E., Lanson, B., Sakharov, B.A., and Drits, V.A. (2005) Investigation of smectite hydration properties by modeling experimental X-ray diffraction patterns: Part I. Montmorillonite hydration properties. *American Mineralogist*, **90**, 1358–1374.
Foster, M.D. (1955) The relation between composition and swelling in clays. *Clays and Clay Minerals*, **3**, 205–220.
Frandsen, C., Legg, B., Comolli, L.R., Zhang, H., Gilbert, B., Johnson, E., and Banfield, J.F. (2014) Aggregation-induced growth and transformation of β-FeOOH nanorods to micron-sized α-Fe_2O_3 spindles. *CrystEngComm*, **16**, 1451–1458.
French, R.H., Müllejans, H., and Jones, D.J. (1998) Optical properties of aluminum oxide: determined from vacuum ultraviolet and electron energy-loss spectroscopies. *Journal of the American Ceramic Society.* **81**, 2549–2557.
Greathouse, J.A., Feller, S.E., and McQuarrie, D. (1994) The modified Gouy-Chapman theory: comparisons between electrical double layer models of clay swelling. *Langmuir*, **10**, 2125–2130.
Grodzinsky, A.J. (2011) *Fields, Forces, and Flows in Biological Systems*. Garland Science
Guthrie, G.D. and Veblen, D.R. (1989) High-resolution transmission electron microscopy of mixed-layer illite/smectite: Computer simulations. *Clays and Clay Minerals*, **37**, 1–11.
Hou, J., Li, H., and Zhu, H. (2009) Determination of clay surface potential: A more reliable approach. *Soil Science Society of America Journal*, **73**, 1658–1663.
Huang, F., Zhang, H.Z., and Banfield, J.F. (2003) The role of oriented attachment crystal growth in hydrothermal coarsening of nanocrystalline ZnS. *Journal of Physical Chemistry B*, **107**, 10470–10475.
Jönsson, B., Labbez, C., and Cabane, B. (2008) Interaction of nanometric clay platelets. *Langmuir*, **24**, 11406–11413.
Klein, W.B. and Oster, J.D. (1982) A model of clay swelling and tactoid formation. *Clays and Clay Minerals*, **30**, 383–390.
Laird, D.A. (2006) Influence of layer charge on swelling of smectites. *Applied Clay Science*, **34**, 74–87.
Legg, B., Zhu, M., Comolli, L.R., Gilbert, B., and Banfield, J.F. (2014) Determination of the three-dimensional structure of ferrihydrite nanoparticle aggregates. *Langmuir*, **30**, 9931–9940.
Li, D., Nielsen, M.H., Lee, J.R.I., Frandsen, C., Banfield, J.F., and De Yoreo, J.J. (2012) Direction-specific interactions control crystal growth by oriented attachment. *Science*, **336**, 1014–1018.
Lifshitz, E.M. (1956) The theory of molecular attractive forces between solids. *Soviet Physics* **2**, 73–83.
Liu, L. (2013) Prediction of swelling pressures of different types of bentonite in dilute solutions. *Colloids and Surfaces A*, **343**, 303–318.
Low, P.F. and Margheim, J.F. (1979) Swelling of clay. 1. Basic concepts and empirical equations. *Soil Science Society of America Journal*, **43**, 473–481.
Luckham, P.F. and Rossi, S. (1999) The colloidal and rheological properties of bentonite. *Advances in Colloidal Science*, **82**, 43–92.
Luef, B., Fakra, S.C., Csencsits, R., Wrighton, K.C., Williams, K.H., Wilkins, M.J., Downing, K.H., Long, P.E., Comolli, L.R., and Banfield, J.F. (2012) Iron-reducing bacteria accumulate ferric oxyhydroxide nanoparticle aggregates that may support planktonic growth. *ISME Journal*, **2012**, 1–13.
Marra, J. (1985) Direct measurements of attractive van der Waals and adhesion forces between uncharged lipid bilayers in aqueous solutions. *Journal of Colloid and Interface Science*, **109**, 11–20.
Miller, S.E. and Low, P.F. (1990) Characterization of the electrical double layer of montmorillonite. *Langmuir* **6**, 572–578.
Missanna, T. and Adell, A. (2000) On the applicability of DLVO theory to the prediction of clay colloids stability. *Journal of Colloid and Interface Science*, **230**, 150–156.
Norrish, K. (1954) Manner of swelling of montmorillonite. *Nature*, **173**, 256–257.
Paineau, E., Bihannic, I., Baravian, C., Philippe, A.-M., Davidson, P., Levitz, P., Funari, S.S., Rochas, C., and Michot, L.J. (2011) Aqueous suspensions of natural swelling clay minerals. 1. Structure and electrostatic interactions. *Langmuir*, **27**, 5562–5573.
Parsegian, V.A. (2006) *Van der Waals Forces.* Cambridge University Press, Cambridge, UK.
Penn, R.L. and Banfield, J.F. (1998) Imperfect oriented attachment: Dislocation generation in defect-free nanocrystals. *Science*, **281**, 969–971.
Penn, R.L., Oskam, G., Strathmann, T.J., Searson, P.C., Stone, A.T., and Veblen, D.R. (2001) Epitaxial assembly in aged colloids. *Journal of Physical Chemistry B*, **105**, 2177–2182.
Podgornik, R. and Parsegian, V.A. (2004) Van der Waals interactions across stratified media. *Journal of Chemical Physics*, **120**, 3401–3405.
Pons, C.H., Rousseaux, F., and Tchoubar, D. (1981) Utilisation du rayonnement synchrotron en diffusion aux petits angles pour l'etude du gonflement des smectites: I. Etude du systeme eau-montmorillonite-Na en fonction de la temperature. *Clay Minerals*, **16**, 23–42.
Quirk, J.P. and Marčelja, S. (1997) Application of double-layer theories to the extensive crystalline swelling of Li-montmorillonite. *Langmuir*, **13**, 6241–6248.
Rajter, R.F., French, R.H., Ching, W.Y., Podgornik, R., and Parsegian, A.V. (2013) Chirality-dependent properties of carbon nanotubes: electronic structure, optical dispersion properties, Hamaker coefficients and van der Waals–London dispersion interactions. *RSC Advances*, **3**, 823–842.
Schuman, D., Hesse, R., Sears, S.K., and Vali, H. (2014) Expansion behavior of octadecylammonium-exchanged low- to high-charge reference smectite-group minerals as revealed by high-resolution transmission electron microscopy on ultrathin sections. *Clays and Clay Minerals* **62**, 336–353.
Schuman, D., Hesse, R., Sears, S.K., and Vali, H. (2014) Expansion behavior of octadecylammonium-exchanged low- to high-charge reference smectite-group minerals as revealed by high-resolution transmission electron microscopy on ultrathin sections. *Clays and Clay Minerals* **62**, 336–353.
Segad, M., Hanski, S., Olsson, U., Ruokolainen, J., Akesson, T., and Jonsson, B. (2012) Microstructural and swelling properties of Ca and Na montmorillonite: (*in situ*) observations with cryo-TEM and SAXS. *Journal of Physical Chemistry C*, **116**, 7596–7601.
Slade, P.G., Quirk, J.P., and Norrish, K. (1991) Crystalline swelling of smectite samples in concentrated NaCl solutions in relation to layer charge. *Clays and Clay Minerals*, **39**, 234–238.

https://doi.org/10.1346/CCMN.2015.0630602 Published online by Cambridge University Press

Svensson, P.D. and Hansen, S. (2013) Combined salt and temperature impact on montmorillonite hydration. *Clays and Clay Minerals*, **61**, 328–341.

Tan, G.L., Lemon, M.F., Jones, D.J., and French, R.H. (2005) Optical properties and London dispersion interaction of amorphous and crystalline SiO_2 determined by vacuum ultraviolet spectroscopy and spectroscopic ellipsometry. *Physical Review B*, **72**, 205117.

Tournassat, C., Ferrage, E., Poinsignon, C., and Charlet, L. (2004) The titration of clay minerals II. Structure-based model and implications for clay reactivity. *Journal of Colloid and Interface Science*, **273**, 234–246.

van Olphen, H. (1977) *An Introduction to Clay Colloid Chemistry.* Interscience Publishers, New York.

Viani, B.E., Low, P.F., and Roth, C.B. (1983) Direct measurement of the relation between interlayer force and interlayer distance in the swelling of montmorillonite. *Journal of Colloid and Interface Science*, **96**, 229–244.

Wilson, J., Cuadros, J., and Cressey, G. (2004) An *in situ* time-resolved XRD-PSD investigation into Na-montmorillonite interlayer and particle rearrangement during dehydration. *Clays and Clay Minerals*, **52**, 180–191.

Yuwono, V.M., Burrows, N.D., Soltis, J.A., and Penn, R.L. (2010) Oriented aggregation: Formation and transformation of mesocrystal intermediates revealed. *Journal of the American Chemical Society*, **132**, 2163–2165.

Zhang, F., Zhang, Z.Z., Low, P.F., and Roth, C.B. (1993) The effect of temperature on the swelling of montmorillonite. *Clay Minerals*, **28**, 25–31.

Zhang, F.S., Low, P.F., and Roth, C.B. (1995) Effects of monovalent, exchangeable cations and electrolytes on the relation between swelling pressure and interlayer distance in montmorillonite. *Journal of Colloid and Interface Science*, **173**, 34–41.

Zhang, H. and Banfield, J.F. (2014) Interatomic Coulombic interactions as the driving force for oriented attachment. *CrystEngComm*, **16**, 1568–1578.

(*Received 24 February 2015; revised 15 January 2016; Ms. 964; AE: M.A. Velbel*)

https://doi.org/10.1346/CCMN.2015.0630602 Published online by Cambridge University Press